Supporting Information:

Inexpensive Thermochemical Energy Storage Utilising Additive Enhanced Limestone

Kasper T. Møller,[1*] Ainee Ibrahim,[1] Craig E. Buckley,[1] Mark Paskevicius[1*]

[1]Physics and Astronomy, Fuels and Energy Technology Institute, Curtin University, GPO Box U1987, Perth 6845, WA, Australia.

*Corresponding Authors
Kasper T. Møller, kasper.moller@curtin.edu.au and Mark Paskevicius, mark.paskevicius@curtin.edu.au

Table S1. Overview of samples investigated.

Primary	Additive	Wt% additive	Mol% additive	Vol% additive	Comments
$CaCO_3$	-	-	-	-	Sigma-Aldrich (SA), ReagentPLUS
$CaCO_3$	C (graphite)	20	67.6	23.0	Hopkins & Williams, 98-99 %
$CaCO_3$	Al_2O_3	10, 20, 40	9.8, 19.7, 39.6	7.1, 14.6, 31.4	SA, Puriss. ≥98 % (bulk); nanopowder, 13 nm (TEM), 99.8 % (nano)
$CaCO_3$	SiO_2	20	29.4	20.3	SA, Nanopowder, 10-20 nm, 99.5 %
$CaCO_3$	Fe_2O_3	20	13.5	11.5	SA, nanopowder, <50 nm
$CaCO_3$	Ni	20	29.9	7.1	SA, <100 nm, ≥99 %
$CaCO_3$	ZnO	20	23.5	10.8	SA, dispersion, 40 wt% in EtOH, <130 nm
$CaCO_3$	ZrO_2	20, 40	16.9, 35.1	10.7, 24.1	SA, nanopowder, <100 nm
$CaCO_3$	Zeolite Y, Na (NaY)	20	13.4	16.9	Alfa Aesar (AA), 900 m/g, 5.1:1 SiO_2:Al_2O_3 molar ratio
$CaCO_3$	Zeolite Y, H (HY)	20	13.4	16.9	AA, 780 m/g, 80:1 SiO_2:Al_2O_3 molar ratio
$CaCO_3$	Zeolite Mordenite, Na (Mor)	20	13.4	16.9	AA, 425 m/g, 13:1 SiO_2:Al_2O_3 molar ratio
$CaCO_3$	$BaCO_3$	9.5	5	6.1	SA, ≥99 %. Deviates from the remainder of the samples due to a previously reported solid-solution regime for $BaCO_3$-$CaCO_3$.[1]

Table S2. Overview of TG-DSC data, cyclic capacity, and reaction products observed after 50 calcination/carbonation cycles at 900 °C and $p(CO_2)_{calcination} \sim 0.7$ bar and $p(CO_2)_{carbonation} \sim 5$ bar.

Primary	Additive	TGA$_{onset}$ [°C]	Mass loss [%]	DSC$_{peak}$ [°C]	Crystalline products after 50 calcination/carbonation cycles	CO$_2$ capacity after 50 calcination/carbonation cycles [%]
CaCO$_3$	-	560	45.2	804 (endo)	CaCO$_3$, CaO	14.8
CaCO$_3$	C (graphite)	610	37.8	845 (endo)	CaCO$_3$, CaO,	19.7
CaCO$_3$	Al$_2$O$_3$ (20 wt%)	630	36.3	830 (endo)	CaCO$_3$, CaO, Ca$_5$Al$_6$O$_{14}$, CaAl$_2$O$_4$, Ca$_3$Al$_2$O$_6$	48.5
CaCO$_3$	SiO$_2$	555	37.6	812 (endo)	CaCO$_3$, CaO, Ca$_5$(SiO$_4$)$_2$CO$_3$	23.0
CaCO$_3$	Fe$_2$O$_3$	590	36.1	820 (endo)	CaCO$_3$, CaO, Fe$_3$O$_4$, Ca$_2$Fe$_2$O$_5$	6.2
CaCO$_3$	Ni	631	31.9	784 (endo)	CaCO$_3$, CaO, Ni	11.1
CaCO$_3$	ZnO	625	39.7	837 (endo)	CaCO$_3$, CaO	5.4
CaCO$_3$	ZrO$_2$ (20 wt%)	612	36.2	843 (endo)	CaCO$_3$, CaO, CaZrO$_3$	52.4
CaCO$_3$	ZrO$_2$ (40 wt%)	610	27.4	810 (endo)	CaCO$_3$, CaO, CaZrO$_3$	35.5
CaCO$_3$	NaY	580	35.7	763 (endo)	CaCO$_3$, CaO, Ca$_5$(SiO$_4$)$_2$CO$_3$	18.2
CaCO$_3$	HY	606	36.7	832 (endo)	CaCO$_3$, CaO, Ca$_5$(SiO$_4$)$_2$CO$_3$	12.9
CaCO$_3$	Mor	635	37.3	836 (endo)	CaCO$_3$, CaO, Ca$_5$(SiO$_4$)$_2$CO$_3$	12.0
CaCO$_3$	0.05 BaCO$_3$	646	41.8	643 (endo), 759 (endo), 851 (endo), 1124 (endo)	CaCO$_3$, CaO, BaCO$_3$, BaCa(CO$_2$)$_3$	7.3

Table S3. Parameters extracted from Rietveld refinement on the *in situ* data of $CaCO_3$-ZrO_2 (40 wt%) sample. The wt% of each compound is given and where possible, crystallite size was extracted and is given in parentheses.

Scan/compound	$CaCO_3$ [wt%] (crystallite size, nm)	CaO [wt%] (crystallite size, nm)	$CaZrO_3$ [wt%] (crystallite size, nm)	ZrO_2 [wt%] (crystallite size, nm)
0	46 (115)	3 (50)	15 (6.7)	36
18 (calcinated)	14 (422)	13 (161)	65 (19.6)	8
32 (carbonated)	28.8 (245)	0.4	65.8 (23)	5
51 (calcinated)	10 (565)	13 (171)	74 (24)	3
63 (carbonated)	26 (227)	0.4	71 (26)	2.6
83 (calcinated)	9	12 (159)	77 (27)	2
94 (carbonated)	25 (234)	0.5	73 (28)	1.5
113 (calcinated)	9.5	12 (147)	77 (29)	1.5
126 (carbonated)	25 (204)	0	73.5 (26)	1.5
146 (calcinated)	9.4	12 (125)	77.4 (27)	1.2
155 (carbonated)	25 (206)	0.5	73.5 (27)	1

Table S4. Specific surface area determined by SAXS for relevant samples.

Sample	Specific Surface Area ($m^2 \cdot g^{-1}$)	CO_2 cycles	Comments
$CaCO_3$	1.9(2)	0	As-milled
$CaCO_3$	4.0(4)	50	Absorbed
$CaCO_3$	3.9(4)	50	Desorbed
$CaCO_3$-Al_2O_3 (20wt%, nano)	29(3)	0	As-milled
$CaCO_3$-Al_2O_3 (20wt%, nano)	3.7(4)	50	Absorbed
$CaCO_3$-Al_2O_3 (20wt%)	3.7(4)	0	As-milled
$CaCO_3$-Al_2O_3 (20wt%)	1.2(1)	50	Absorbed
$CaCO_3$-Al_2O_3 (20wt%)	1.2(1)	500	Absorbed
$CaCO_3$-ZrO_2 (40wt%)	52(5)	0	As-milled
$CaCO_3$-ZrO_2 (40wt%)	3.1(3)	50	Absorbed
$CaCO_3$-ZrO_2 (40wt%)	4.7(5)	100	Absorbed

Thermal Analysis

TG-DSC data of the samples reveal that the $CaCO_3$ in all cases decomposes between 763 – 851 °C under argon flow, see Figure S1, S2 and Table S2. This is a positive observation, as a high decomposition temperature is sought and thus destabilisation of the material is not preferable. The as-milled $CaCO_3$ has an endothermic DSC peak signal at 804 °C, which is in the middle of the observed decomposition range. A slight destabilisation in the NaY sample is probably due a reaction between SiO_2 (in the zeolite structure) and $CaCO_3$ to form spurrite, $Ca_5(SiO_2)_4CO_3$, according to reaction scheme S1:

$$5CaCO_3 + 2SiO_2 \rightarrow Ca_5(SiO_4)_2CO_3 + 4CO_2 \qquad (S1)$$

(c.f. the results on powder X-ray diffraction). However, as the NaY sample decomposes earlier than the purely added SiO_2 sample the destabilisation is assigned to the Al_2O_3. Contrary to this, the thermal stability of, e.g. $BaCO_3$ ($T_{dec} > 1100$ °C) seems to increase the decomposition temperature to 851 °C. Finally, small differences in particle size as a function of ball-milling may also cause the minor differences observed.
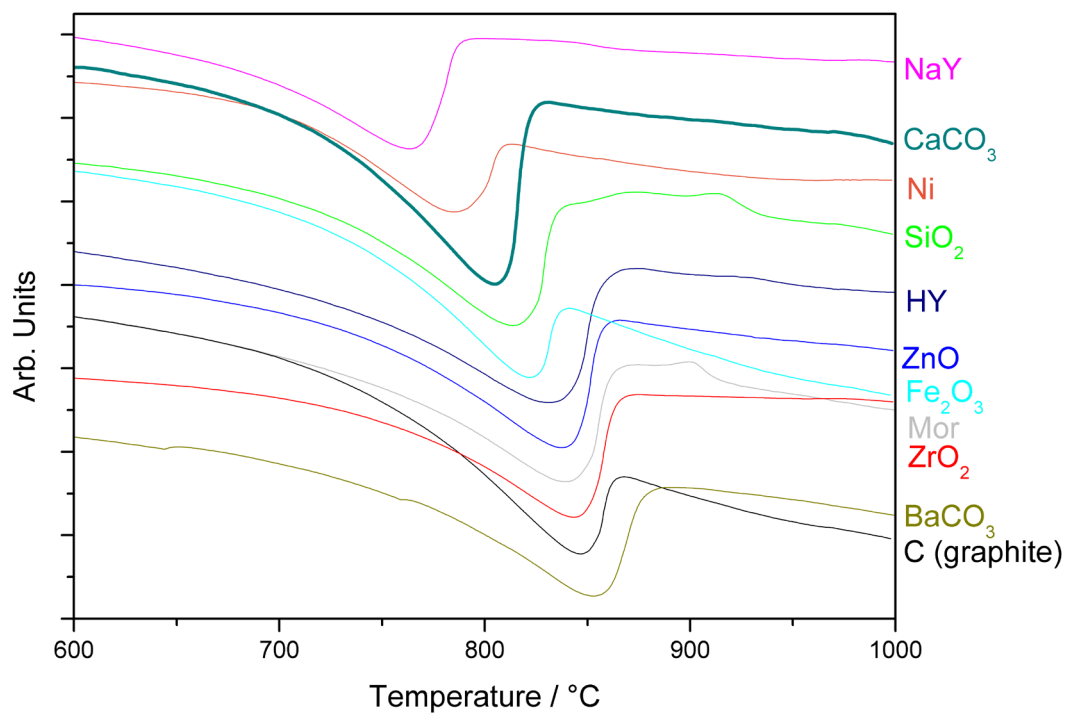
Figure S1. Comparison of the DSC data between 600 and 1000 °C of the investigated samples, which show that the samples generally decompose within the temperature range 763 – 851 °C.
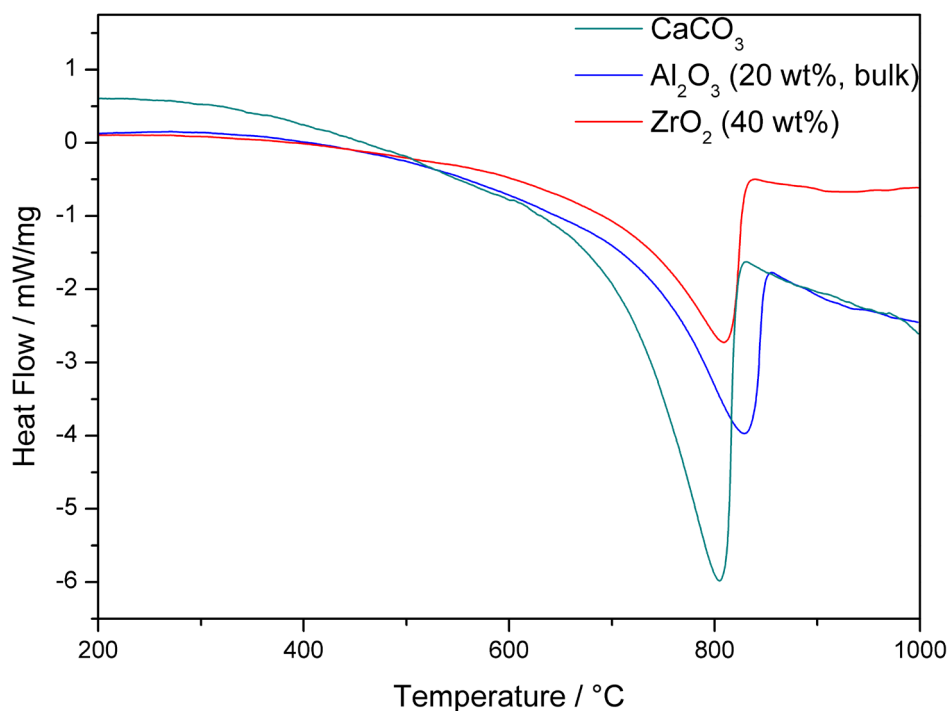
Figure S2. Comparison of the DSC data for the most promising samples containing $CaCO_3$-Al_2O_3 (20 wt%) and $CaCO_3$-ZrO_2 (40 wt%).
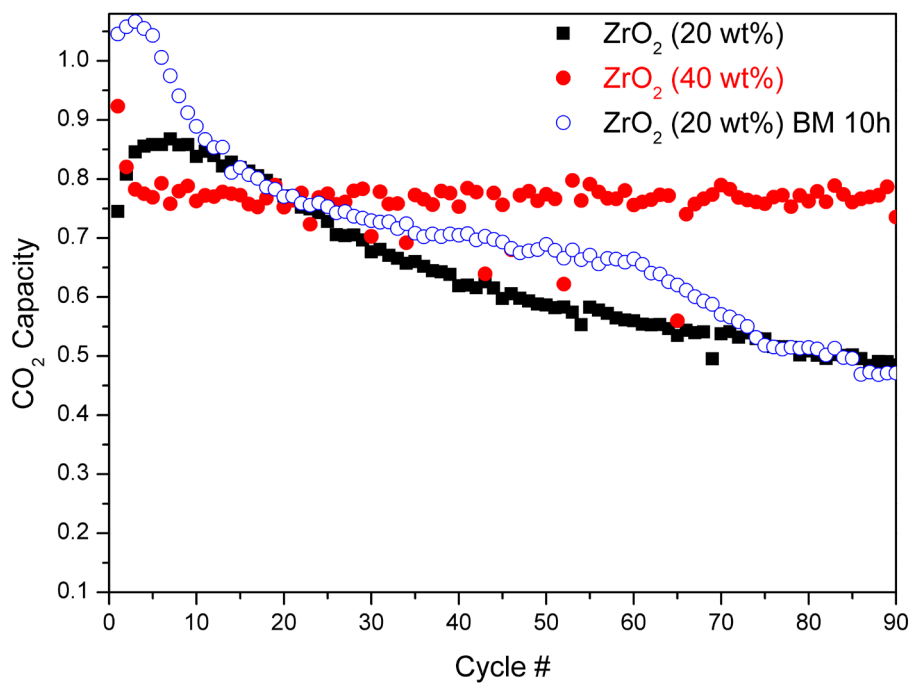
Figure S3. Absorption data comparing the influence of ZrO_2 content and ball-milling parameters over 90 calcination-carbonation cycles. The data has been corrected for reacted material to form $CaZrO_3$. Hence, when adding 20 or 40 wt% ZrO_2, 69 or 32 wt% $CaCO_3$, respectively, will be left after the reaction, which is then set as 100 %, *i.e.* 1 mol of CO_2.
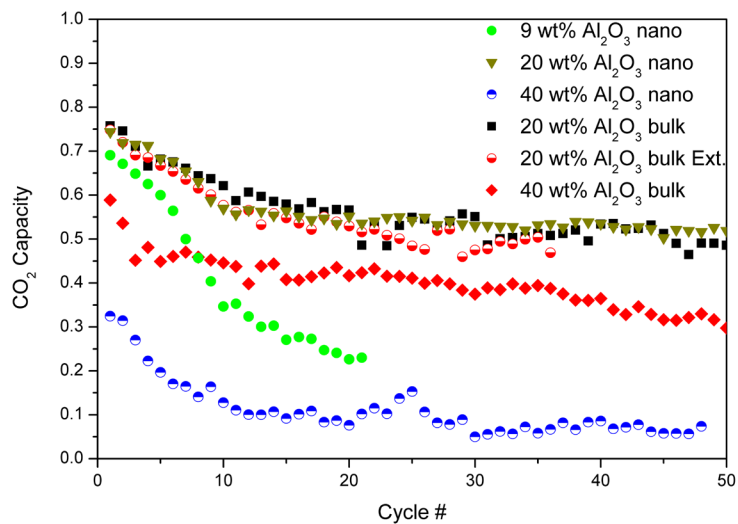
Figure S4. Absorption data comparing the influence of Al_2O_3 content, initial particle size, and extended calcination/carbonation time (1h/1h) up to 50 calcination-carbonation cycles.
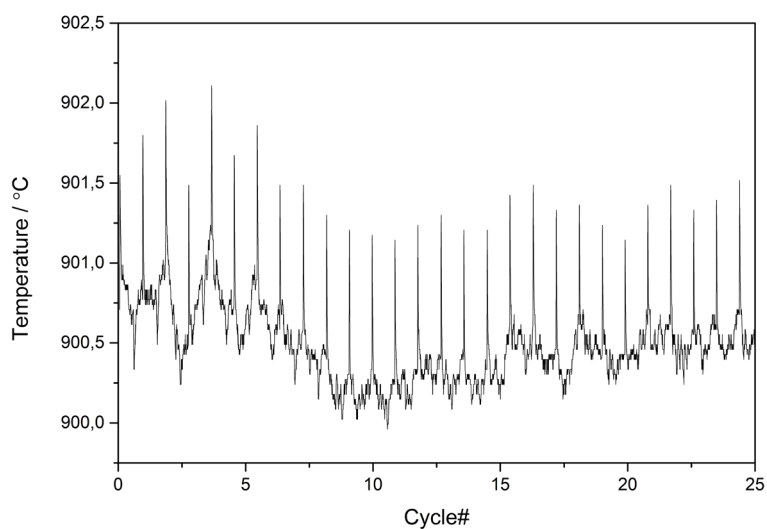
Figure S5. Temperature data on $CaCO_3$-Al_2O_3 (20 wt%) during the first 25 CO_2 cycles highlighting especially the temperature increase on CO_2 absorption (carbonation).

Reaction kinetics
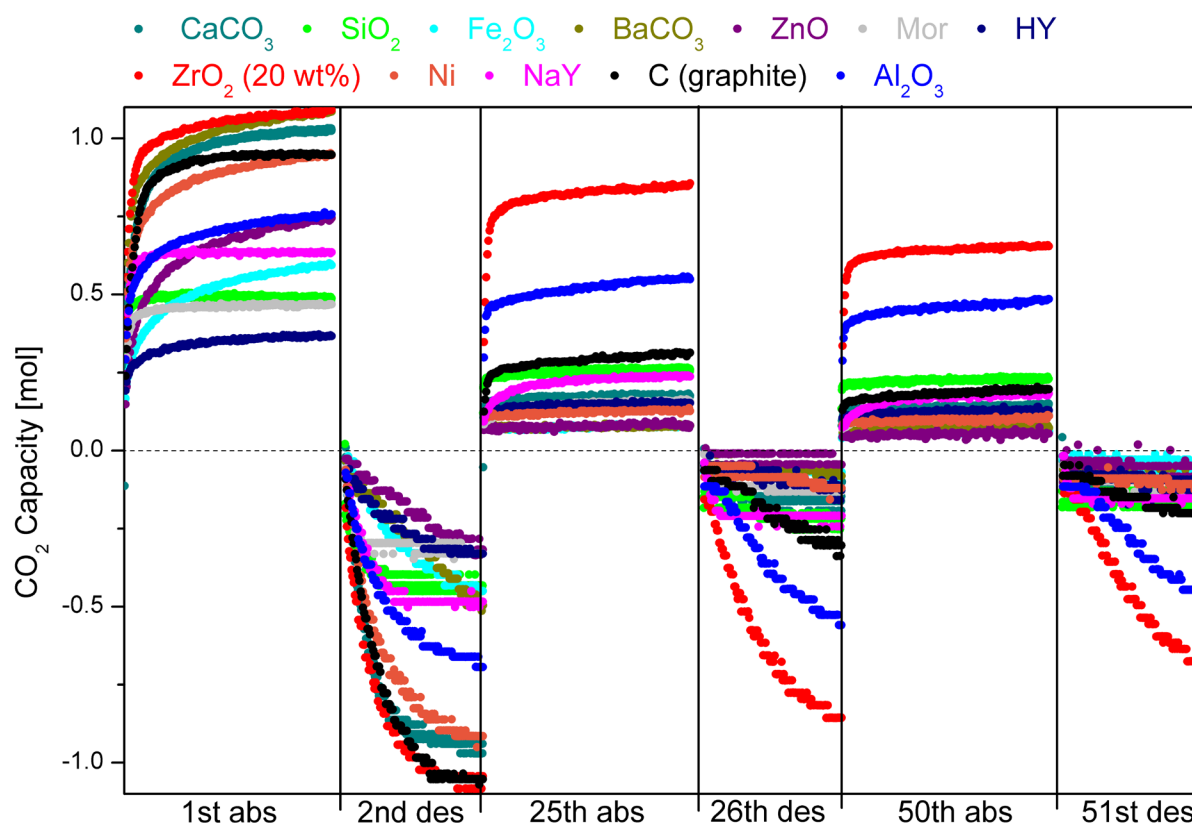
Figure S6. Comparison of the calcination/carbonation kinetics of all samples at the initial, middle, and final stage of the 50 cycles. The calcination/carbonation (des/abs) cycle is given on the *x*-axis.

During the first absorption and second desorption the pristine $CaCO_3$, ZrO_2, graphite, and Ni samples possess the fastest reaction kinetics. The $BaCO_3$ sample show a fast first absorption, but the following desorption kinetics are very slow. After 25 cycles, it is clear that the ZrO_2 (20 wt%) is superior to the remaninder of the samples. However, the graphite and SiO_2 samples also demonstrate fast kinetics, but a low overall capacity. In the 50th cycle, it is noteworthy how the desorption kinetics of the ZrO_2 (20 wt%) sample has decreased, whereas the absorption kinetics remain fast (~95 % of the reached capacity within 3.5 minutes). For the remainder of the series, the absorption kinetics seem to be fast as a plateua, limited by the capacity, is reached within 10 minutes for all of them. However, desorption seems to be slow. Generally, the desorption kinetics are slower compared to absorption. The latter makes a build-up of $CaCO_3$ possible. However, as identified from PXD (cf. Powder X-ray Diffraction), CaO is a main component in the samples after the final absorption measurement.

Powder X-ray Diffraction
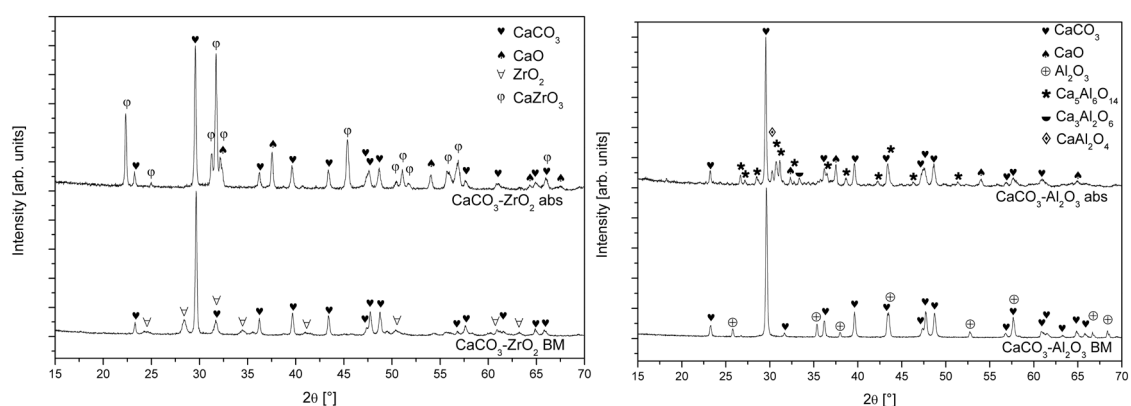
Figure S7. PXD data of *left*: CaCO₃-ZrO₂ (20 wt%) and *right*: CaCO₃-Al₂O₃ (20 wt%) of the as-milled and absorbed samples after 50 calcination/carbonation cycles showing the formation of ternary compounds.

After 50 absorption/desorption cycles reveal that CaO is present after the attempt to absorb CO_2, hence explaining the decreasing CO_2 capacity of the samples. However, multiple reactions are also observed between the $CaCO_3$ and the additive, *i.e.* in the cases of $BaCO_3$, Fe_2O_3, SiO_2, Zeolite Y, Zeolite Mordenite, and C (graphite):

$$BaCO_3(s) + CaCO_3(s) \rightarrow BaCa(CO_3)_2(s) \qquad (S2, \text{ref } [2])$$

$$CaCO_3(s) + C(s) \rightarrow CaO(s) + 2CO(g) \qquad (S3, \text{ref } [3])$$

$$5CaCO_3(s) + 2SiO_2(s) \rightarrow Ca_5(SiO_4)_2CO_3(s) + 4CO_2(g) \qquad (S4, \text{refs } [4,5])$$

$$2CaO(s) + Fe_2O_3(s) \rightarrow Ca_2Fe_2O_5(s) \qquad (S5, \text{ref } [6])$$
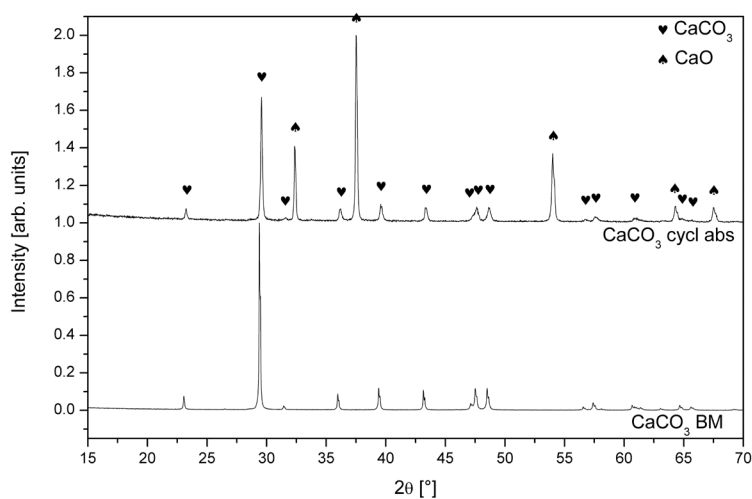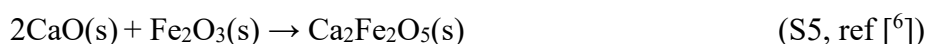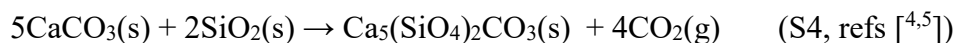
Figure S8. PXD data of as-prepared and after 50 calcination/carbonation cycles ending in the absorbed state of the $CaCO_3$ sample.
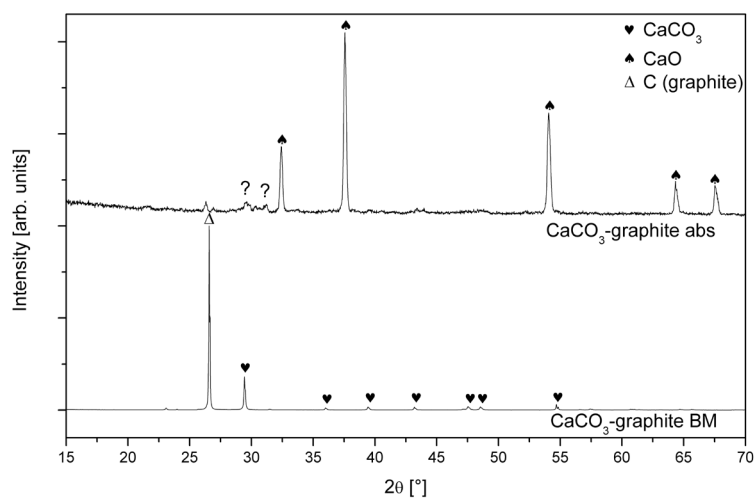
Figure S9. PXD data of as-prepared and after 50 calcination/carbonation cycles ending in the absorbed state of the CaCO₃-Graphite sample.
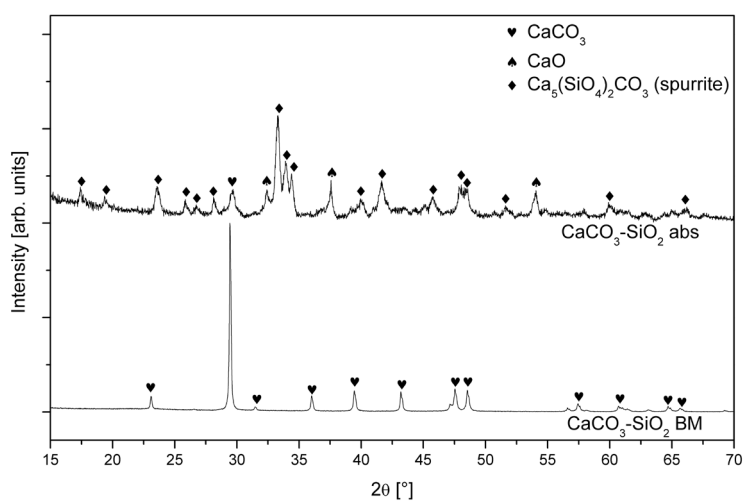
Figure S10. PXD data of as-prepared and after 50 calcination/carbonation cycles ending in the absorbed state of the CaCO₃-SiO₂ sample.
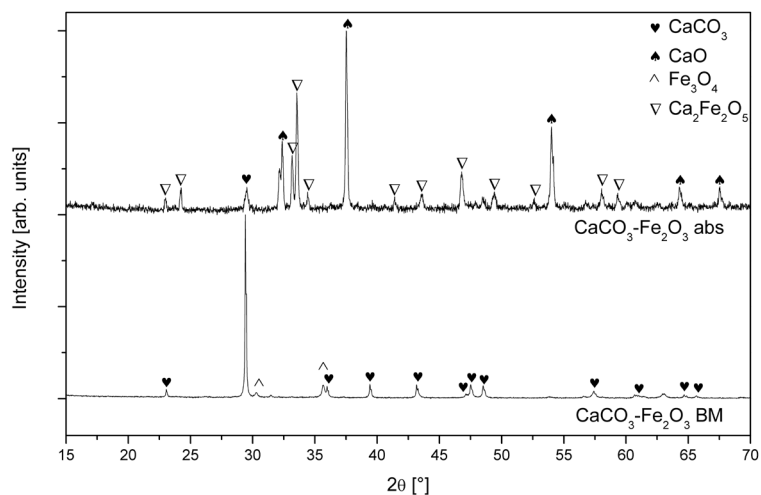
Figure S11. PXD data of as-prepared and after 50 calcination/carbonation cycles ending in the absorbed state of the CaCO₃-Fe₂O₃ sample.
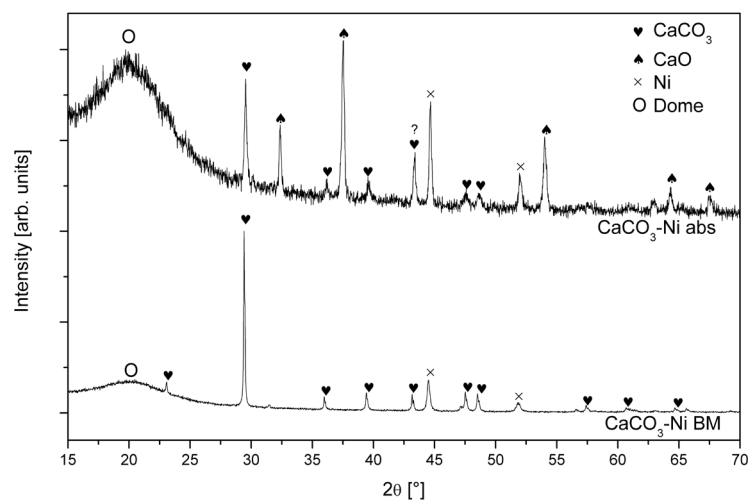
Figure S12. PXD data of as-prepared and after 50 calcination/carbonation cycles ending in the absorbed state of the CaCO₃-Ni sample.
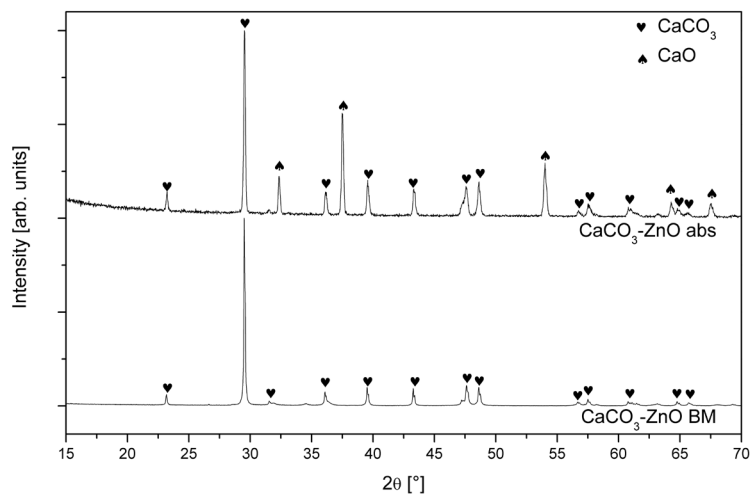
Figure S13. PXD data of as-prepared and after 50 calcination/carbonation cycles ending in the absorbed state of the CaCO₃-ZnO sample.
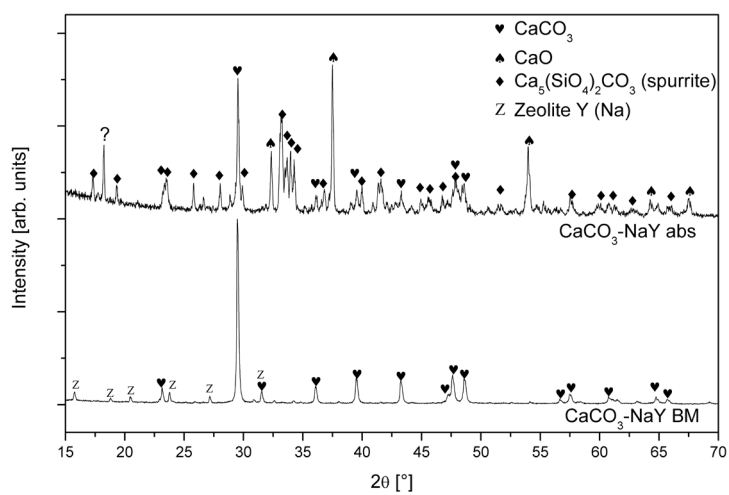
Figure S14. PXD data of as-prepared and after 50 calcination/carbonation cycles ending in the absorbed state of the CaCO₃-Zeolite Y (Na) sample.
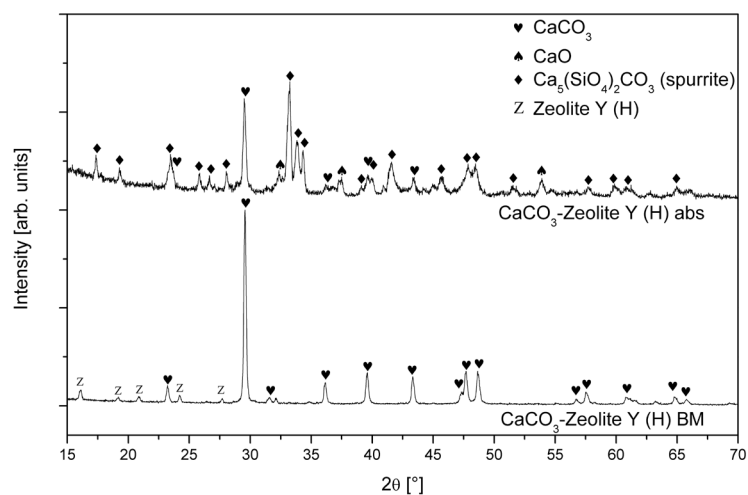
Figure S15. PXD data of as-prepared and after 50 calcination/carbonation cycles ending in the absorbed state of the CaCO$_3$-Zeolite Y (H) sample.
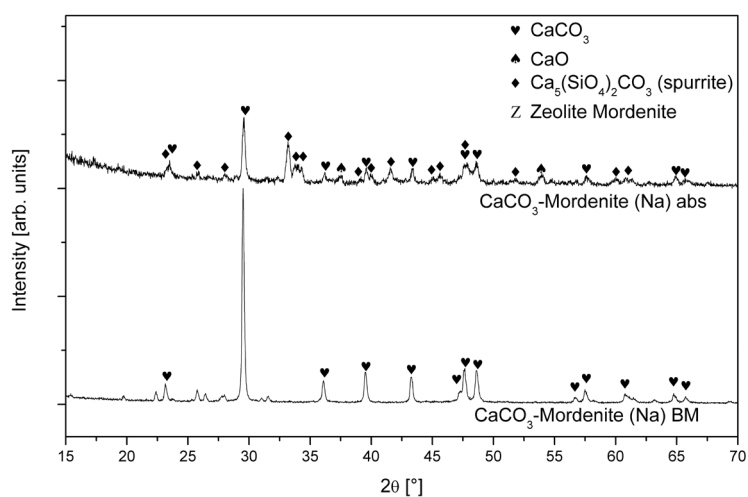
Figure S16. PXD data of as-prepared and after 50 calcination/carbonation cycles ending in the absorbed state of the CaCO$_3$-Mordenite (Na) sample.
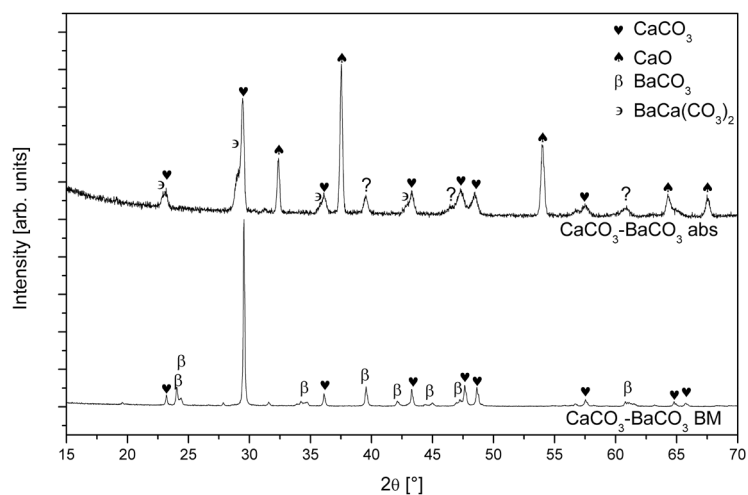
Figure S17. PXD data of as-prepared and after 50 calcination/carbonation cycles ending in the absorbed state of the $CaCO_3$-$BaCO_3$ sample.
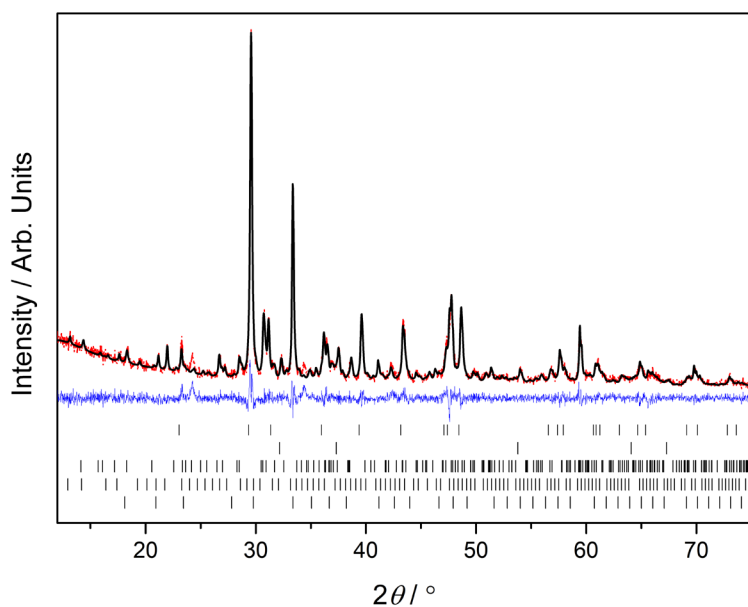
Figure S18. Rietveld refinement on PXD data on $CaCO_3$-Al_2O_3 (20 wt%) at room temperature after 500 CO_2 cycles. Y_{obs}: red; Y_{calc}: black, and Y_{diff}: blue. *hkl* markers (bottom singular markers) from top to bottom: $CaCO_3$, CaO, $Ca_5Al_6O_{14}$, $Ca_9Al_6O_{18}$ and $Ca_{12}Al_{14}O_{33}$. R_{wp} = 10.467 %.
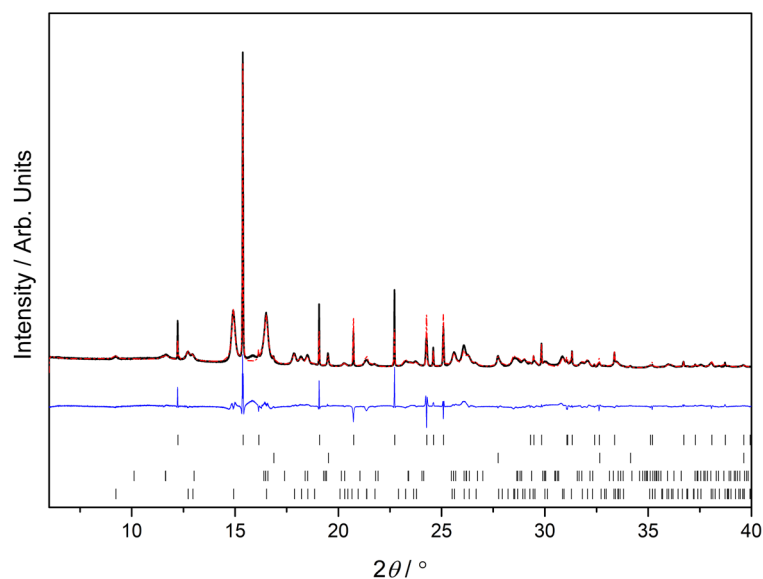
Figure S19. Rietveld refinement on *in situ* SR PXD data on CaCO$_3$-ZrO$_2$ (40 wt%) at T = 900 °C and t ~ '0' min. Y_{obs}: red; Y_{calc}: black, and Y_{diff}: blue. *hkl* markers (bottom singular markers) from top to bottom: CaCO$_3$, CaO, CaZrO$_3$, and ZrO$_2$. R_{wp} = 9.881 %.
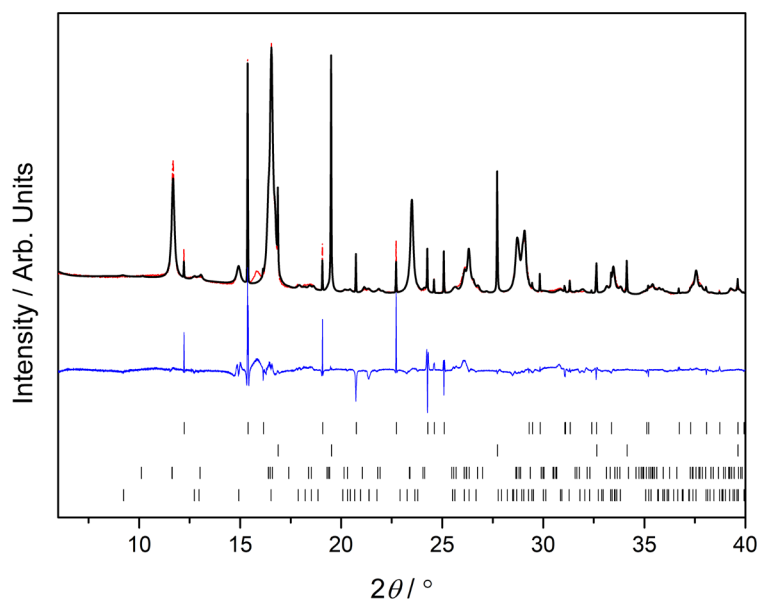
Figure S20. Rietveld refinement on *in situ* SR PXD data on CaCO$_3$-ZrO$_2$ (40 wt%) at T = 900 °C and t ~ 25 min. Y_{obs}: red; Y_{calc}: black, and Y_{diff}: blue. *hkl* markers (bottom singular markers) from top to bottom: CaCO$_3$, CaO, CaZrO$_3$, and ZrO$_2$. R_{wp} = 7.863 %.
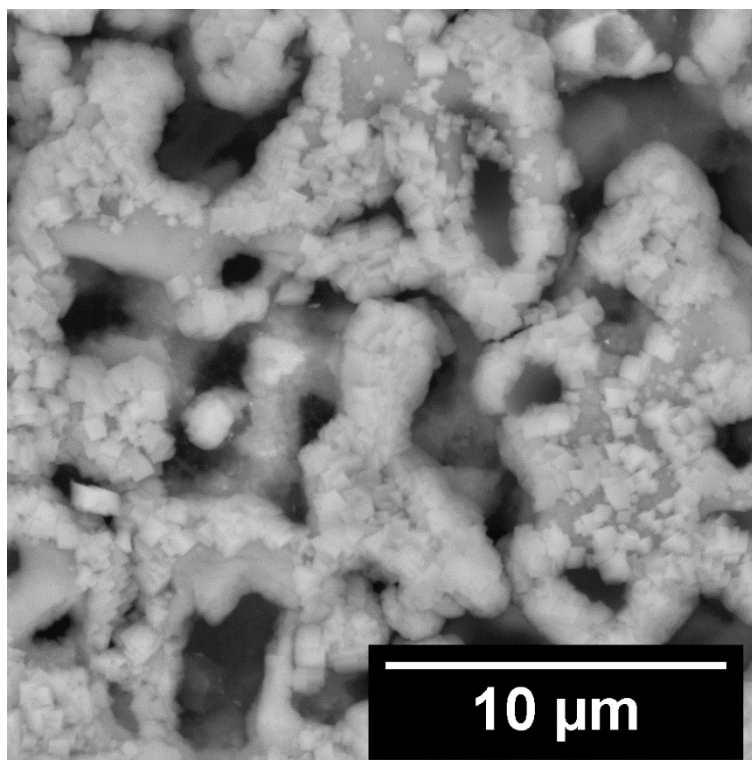
Figure S21. SEM image of neat $CaCO_3$ cycled 50 times, highlighting the small particles present on the surface of a 'worm'-like morphology structure.
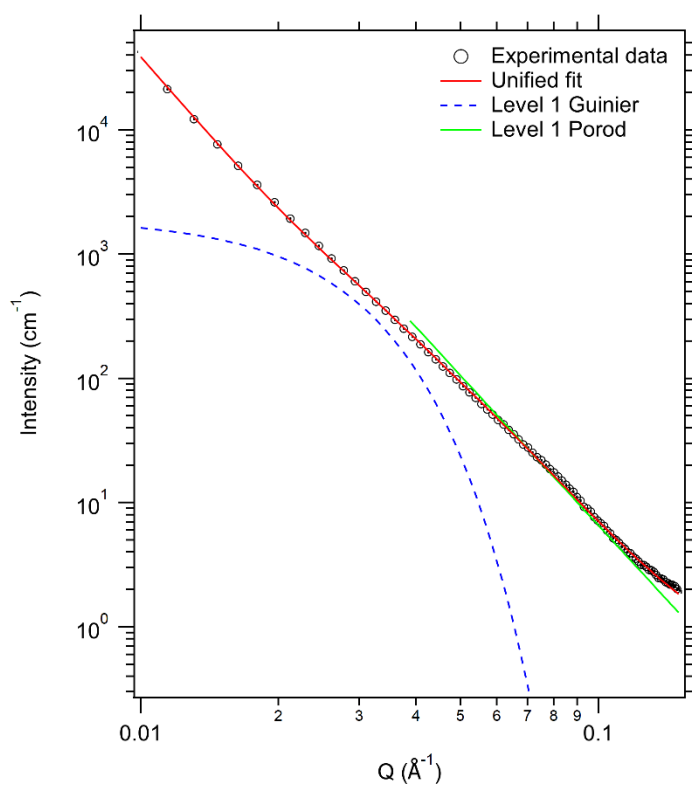
Figure S22. Representative fit to SAXS data using the Unified model for $CaCO_3$ 50 cycles (des). The Guinier and Porod (slope = -4) regions are shown for Level 1, from where the specific surface area (SSA) was determined.
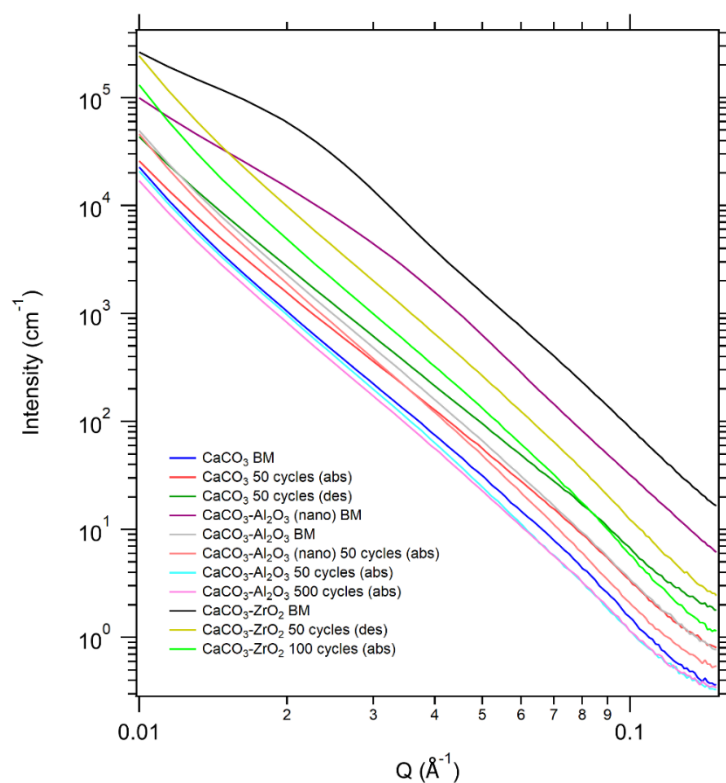
Figure S23. SAXS data for ballmilled (BM) and cycled materials in the absorbed (abs) or desorbed (des) state.

References

1 L. L. Y. Chang, *J. Geol.*, 1965, **73**, 346–368.
2 A. Grandjean and G. Leturcq, *J. Nucl. Mater.*, 2005, **345**, 11–18.
3 Y. Kashiwaya, R. Suzuki and K. Ishii, *ISIJ Int.*, 2011, **51**, 1213–1219.
4 H. Bolio-Arceo and F. P. Glasser, *Cem. Concr. Res.*, 1990, **20**, 301–307.
5 F. P. Glasser, *Cem. Concr. Res.*, 1973, **3**, 23–28.
6 M. Ismail, W. Liu, M. S. C. Chan, M. T. Dunstan and S. A. Scott, *Energy Fuels*, 2016, **30**, 6220–6232.